Raman and infrared studies of Sr_2TiO_4: A material isomorphic to $(La,Sr)_2CuO_4$ superconductors

Gerald Burns and F. H. Dacol
IBM Thomas J. Watson Research Center, P.O. Box 218, Yorktown Heights, New York 10598

G. Kliche and W. König
Max-Planck-Institut für Festkörperforschung, Heisenbergstrasse 1, D-7000 Stuttgart 80, Federal Republic of Germany

M. W. Shafer
IBM Thomas J. Watson Research Center, P.O. Box 218, Yorktown Heights, New York 10598

(Received 13 October 1987)

The high-temperature superconductor $(La_{2-x}Sr_x)CuO_4$ has the K_2NiF_4 structure, as does Sr_2TiO_4. In order to understand better the phonon spectra obtained from ceramic $(La_{2-x}Sr_x)CuO_4$, we have performed Raman and infrared measurements on ceramic, insulating Sr_2TiO_4. All four Raman-allowed phonons are observed and found to be quite sharp, because in this centrosymmetric structure the Raman-mode frequencies are isotropic. The infrared reflectivity spectra are more difficult to interpret because reststrahlen bands are measured, which extend from the transverse-optic (TO) frequency to the longitudinal-optic (LO) frequency. Symmetry forbids overlap of the $3A_{2u}$ bands as well as the $4E_u$ bands. The interpretation, nevertheless, is difficult because the A_{2u} and E_u bands can overlap one another. By comparison with single-crystal results in fluorides and chlorides having the same structure we have been able to identify many of the infrared modes in our spectra. This knowledge permits a determination of most of the infrared active modes in $(La_{2-x}Sr_x)CuO_4$. In the superconductor, two other effects aid our understanding of the spectra. (a) The effective charges are smaller than in Sr_2TiO_4, reducing the TO-LO splitting, and thus the overlap of the reflectivity bands. (b) The electron plasma is confined to the xy plane, and consequently it interacts strongly only with the E_u phonons, and leaves the A_{2u} phonons largely unaffected.

I. INTRODUCTION

Since the discovery of high-temperature superconductivity in (La, Ba, Sr)$_2$CuO$_4$-type materials[1] there has been a huge research effort on these and the related $YBa_2Cu_3O_7$ superconductors.[2,3] Of course, electron-phonon coupling is a central issue in the theory of superconductivity.[4] Thus, it is natural to study the phonons in these systems with Raman, infrared, and neutron techniques, although it is possible that high-temperature superconductivity in these oxides is not phonon meditated.[2,3]

These high-temperature superconducting oxides have been generally available only in the form of polycrystalline ceramics. Thus, neutron techniques yield only the density of phonon states.[5] However, Raman and infrared measurements, which measure the zone center ($k \approx 0$) phonons, can be used to determine these phonon frequencies. For Raman-active phonons in a centrosymmetric material, the frequencies do not depend on the angles between the phonon propagation direction and the crystallographic directions. Thus, sharp phonon lines can be measured in ceramic samples, but the selection rules cannot be used to sort out the irreducible representations of the various phonons. In noncentrosymmetric crystals, where the Raman phonon frequencies do depend on the various angles, the angular dependence can be exploited to yield the phonon frequencies.[6] In noncubic crystals, the frequencies of infrared-active modes depend on the various angles of incidence.[7] In analogy with the Raman technique, we demonstrate that data from ceramics can be used to obtain the infrared-active modes. By performing both Raman and infrared measurements on materials that are insulators, but with the same crystal structures as the high-temperature superconductors, we are able to interpret the experimental results,[8-10] and to determine the phonon frequencies in $(La_{2-x}Sr_x)CuO_4$.

II. EXPERIMENTAL PROCEDURE

Following previous work,[11,12] the samples were prepared by reacting titanium dioxide with the alkaline-earth carbonates. They were first reacted at 950 °C for 12 h, then reground and heated to 1275 °C for 18 h. The poorly sintered powders were then ground thoroughly, pressed into pellets, fired in oxygen at 1600 °C for 20 h, and then cooled to room temperatures at ≈ 50 °C/h. Some samples were annealed at 1250 °C in oxygen for several days, but these gave similar experimental results. As determined by x-ray diffraction, the materials were single phase with the K_2NiF_4 structure, containing less than 5% of the $Sr_3Ti_2O_7$ phase.

The Raman results were measured on a standard double monochrometer using an argon-ion laser operating at 5145 and 4880 Å. The infrared measurements were carried out on a Bruker Fourier-Spectrometer IFS 113v with a resolution of 2 cm^{-1}. An aluminum mirror was used as a reference.

III. STRUCTURE AND SYMMETRY CONSIDERATIONS

Both Sr_2TiO_4 and the $(La,Sr)_2CuO_4$-type superconductors crystallize in the tetragonal K_2NiF_4 structure,[13] whose generic formula can be written as A_2BO_4. The space group is $I4/mmm(D_{4h}^{17})$, with $z=2$, and the primitive unit cell contains one formula unit.[13-15] The structure is shown in Fig. 1, and the positions of the atoms are given in Table I, part (a). Group theory predicts 7 infrared- and 4 Raman-active modes for this structure type [Table I, parts (b) and (c)]. From the symmetry-adapted vectors [Table I, part (b)], obtained using projection operator techniques,[14] we see that in the Raman-active E_g mode, the two O_z atoms (as well as the A atoms) move in opposite directions along the x axis (i.e., x_4-x_3). Likewise the motion can be along the y axis. For the silent mode the O_x and the O_y atoms move parallel to the z axis in the opposite directions (i.e., z_2-z_3). The normal modes are linear combinations of the symmetry-adapted vectors that transform as the same irreducible representations. Of course, using a model for the short- and long-range interatomic potentials, the normal modes themselves can be calculated, and they will be discussed later.

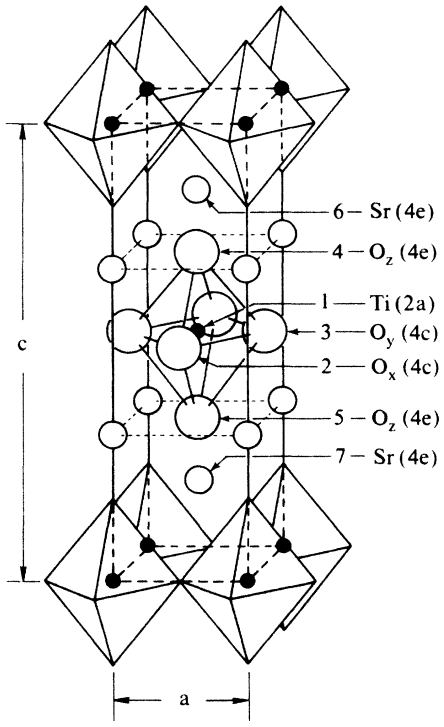

FIG. 1. The multiprimitive unit cell for Sr_2TiO_4 which has the K_2NiF_4 structure. The positions of the seven atoms in the primitive unit cell are shown along with the Wyckoff notation for their sites. The seven atoms are labeled 1 to 7, in an arbitrary manner for future use.

TABLE I. Various symmetry results for A_2BO_4 with the K_2NiF_4 structure, space group $I4/mmm(D_{4h}^{17})$.

(a) Atomic positions		
B atoms	$2a$	(000), $(\frac{1}{2},\frac{1}{2},\frac{1}{2})$
O_x and O_y atoms	$4c$	$(0,\frac{1}{2},0)$, $(\frac{1}{2},0,0)$, $(\frac{1}{2},0,\frac{1}{2})$, $(0,\frac{1}{2},\frac{1}{2})$
A atoms	$4e$	$(0,0,z)$, $(0,0,\bar{z})$, $(\frac{1}{2},\frac{1}{2},\frac{1}{2}+z)$, $(\frac{1}{2},\frac{1}{2},\frac{1}{2}-z)$ $z\approx 0.35$
O_z atoms	$4e$	Same, with $z\approx 0.15$
(b) Classification of the normal modes		
B atoms	$2a$	A_{2u} z_1
		E_u x_1,y_1
O_x and O_y atoms	$4c$	A_{2u} z_2+z_3
		B_{2u} z_2-z_3
		$2E_u$ x_2,y_2 x_3,y_3
A atoms	$4e$	A_{1g} z_6-z_7
		E_g x_6-x_7, y_6-y_7
		A_{2u} z_6+z_7
		E_u x_6+y_7, y_6+y_7
O_z atoms	$4e$	$A_{1g}+E_g+A_{2u}+E_u$ Same symmetry coordinates as A atoms but with z_4-z_5, etc.
(c) The sum of the modes grouped according to type of activity		
$A_{2u}+E_u$	Acoustic	
$3A_{2u}+4E_u$	ir	
$2A_{1g}+2E_g$	Raman	
B_{2u}	Silent	

IV. RESULTS

A. Raman

Figure 2 shows the low-temperature Raman spectra for Sr_2TiO_4, as well as the two closely related materials, as labeled. The four first-order Raman lines expected from the group theory (Table I) are labeled 1 to 4. Let us first discuss the features labeled *i*. From x-ray measurements we find about 5% of Sr_2TiO_4 in $Sr_3Ti_2O_7$ and vice versa. The Raman modes from these impurities can be seen at room temperature[8] but become sharper and more apparent at low temperature. These impurity lines are labeled *i* and the frequencies correspond exactly to those found in the related materials.

A surprising feature of the Raman-active modes in Sr_2TiO_4 is that some of them are very sharp at low temperatures, even in these ceramic samples. The linewidths and positions found in Sr_2TiO_4 are given in Table II, part (a). For crystals with a structure that has a center of symmetry, the exclusion principle[14] requires that the Raman modes may not be simultaneously infrared active. Thus, the Raman-mode frequencies do not vary with the angle between their propagation direction (*k* direction) and crystallographic axis,[6] giving a natural explanation for the observed narrow linewidths.

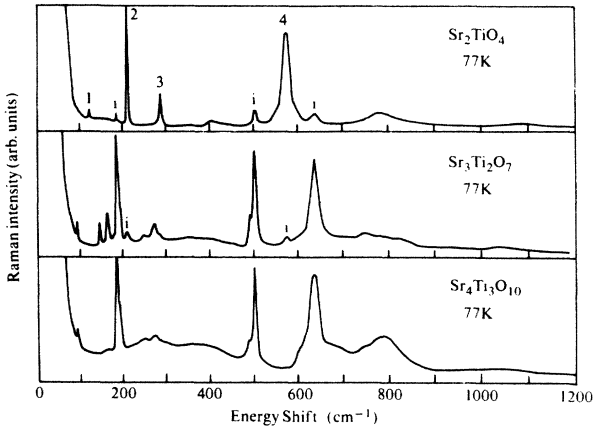

FIG. 2. The Raman spectra, at 77 K, of Sr_2TiO_4 as well as two closely related compounds, as indicated (Ref. 8). The four Raman-allowed modes are labeled 1 to 4. See the text for the meaning of the modes labeled *i*.

B. Infrared frequencies

The positions of the infrared modes, in contrast, do vary with the angle between the infrared electric field vector, E, and the crystallographic *c* axis.[6,7] Because of this angular dependence, it is worthwhile to discuss what should be observed in a ceramic material in reflectivity measurements. Such measurements are shown in Fig. 3(a) for Sr_2TiO_4. Let θ be the angle between the *E* vector of the infrared radiation and the crystallographic *c* axis. The angular dependence is very similar to that of Raman-active modes that are simultaneously infrared active.[6] Figure 4 shows a schematic diagram of the θ dependence

TABLE II. (a) The positions and linewidths of the phonon modes in Sr_2TiO_4 at room temperature and 77 K. For the mode assignments, see the text. (b) The frequencies and mode assignments for the various infrared-active modes. See the text for a discussion of how these modes are assigned. (c) The modes obtained for $(La_{2-x}Sr_x)CuO_4$, as discussed in the text.

(a) Phonon modes in Sr_2TiO_4

	Position		Linewidth	
	RT	77 K	RT	77 K
1	123.9	123.2	4.6	1.3
2	205.4	207.2	3.9	1.7
3	286.2	285.9	15.6	3.5
4	578.3	573.2	40.1	21.5

(b) Frequency and mode assignments

Freq.	Type	Freq.	Type
151	E_u(TO)	182	E_u(LO)
197	E_u(TO)	239	E_u(LO)
≈242	A_{2u}(TO) or E_u(TO)		
≈259	E_u(TO) or A_{2u}(TO)	≈467	A_{2u}(LO) and E_u(LO)
545	A_{2u}(TO)	≈685	A_{2u}(LO)
		727	E_u(LO)

(c) Modes for $(La_{2-x}Sr_x)CuO_4$

Freq.	Type	Freq.	Type
117	E_u(TO)	≈140	E_u(LO)
232	A_{2u}(TO)	(340)	A_{2u}(LO)
350	A_{2u}(TO)	460	A_{2u}(LO)
510	A_{2u}(TO)	544	A_{2u}(LO)
672	E_u(TO)	691	E_u(LO)

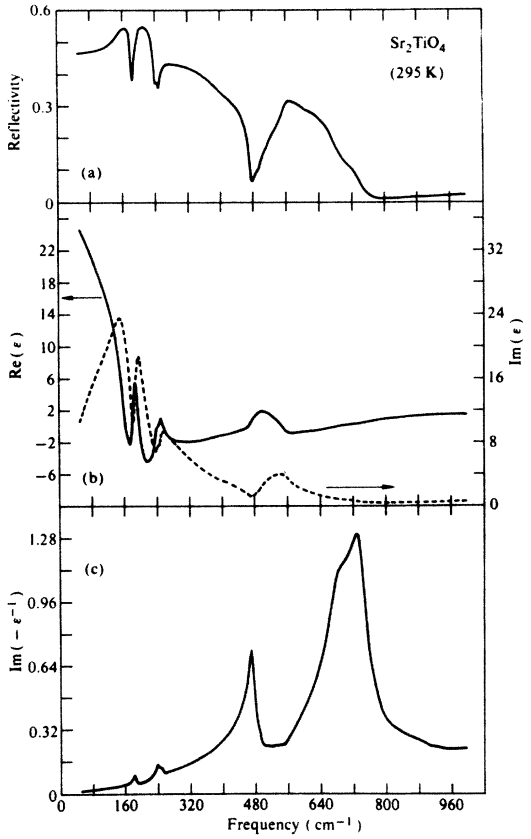

FIG. 3. (a) The frequency dependence of the reflectivity of Sr_2TiO_4. (b) The real and imaginary part of the dielectric constant obtained by a Kramers-Kronig analysis of the reflectivity data. (c) A plot of $\mathrm{Im}(-\epsilon^{-1})$ vs frequency.

of the infrared-active modes.[7] In single crystals in which reflectivity has been measured as a function of θ, good agreement with experiment has been found.[7]

Ceramics consist of small crystals of all orientations. Thus, when a response function, such as reflectivity is measured, the angular dependence of the mode frequencies (Fig. 4) must be taken into account. For any value of θ, the crystal has normal modes, but it is only at the extreme ($\theta=0$ and $\pi/2$) that the modes are called "the" modes with the labels $E_u(\mathrm{TO})$, $A_{2u}(\mathrm{TO})$, $A_{2u}(\mathrm{LO})$, and

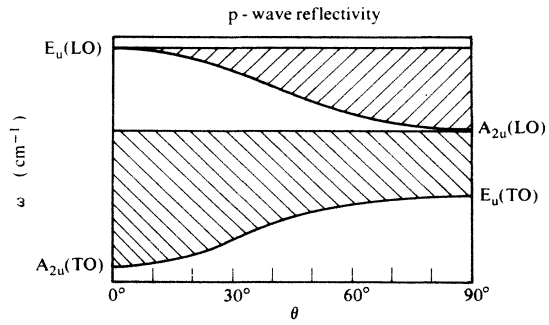

FIG. 4. A schematic of the angular dependence of a reststrahlen band for p-wave polarization (Ref. 7).

$E_u(\mathrm{LO})$, as indicated in Fig. 4. At other angles the modes are called quasimodes. Furthermore, Fig. 4 only applies to p polarization, where the E vector is in the plane containing the incoming and reflected light, and the c axis. For s polarization (E perpendicular to this plane) only $E_u(\mathrm{TO})$ and $E_u(\mathrm{LO})$ modes are measured, independent of θ. As in the Raman case,[6] small crystallites near the extreme ($\theta=0$ and $\pi/2$) give the predominant contribution to observed signals because the smallest angular dependence of the frequency occurs for such crystals. In other words, the number of crystallites with responses in a certain energy range is largest whenever the energy versus θ has extremes.

For the infrared response from ceramic samples, we expect to observe the modes in a similar way as has been observed in Raman spectra.[6] However, in noncubic materials the reststrahlen bands that transform as different irreducible representation can overlap each other in some frequency regions. In Fig. 5, the work by Geick and others[16–21] on the fluorides and chlorides of materials with the K_2NiF_4 structure are summarized. We have connected the TO to LO mode as in a bar graph to represent a reststrahlen reflectivity band. For a series of modes transforming as the same irreducible representations the

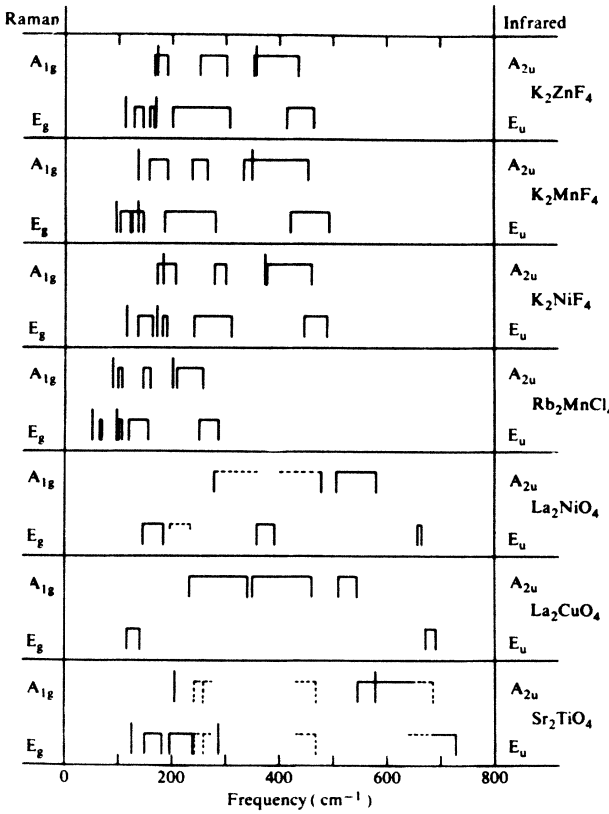

FIG. 5. The frequencies for various bands and modes for the materials as listed. The simple vertical lines represent Raman modes either of A_{1g} or E_g type, as indicated on the left. The bars represent infrared reflectivity bands of A_{2u} or E_u type, as indicated on the right. The lower-energy side of the reflectivity band corresponds to the TO mode and the higher energy to the LO mode. Dashed lines represent uncertainties.

reststrahlen bands cannot overlap in frequency. For example, this can be seen for the E_u bands in Fig. 5, and also separately for the A_{2u} bands. However, there are frequency regions where the A_{2u} bands overlap the E_u bands, and this gives rise to the problem of interpreting the spectra measured in ceramics.

Using the single-crystal fluoride and chloride results shown in Fig. 5, we can predict what we expect to see in a ceramic material. In the high-frequency region, in the fluorides and chlorides the highest frequency A_{2u} and E_u modes always have the same characteristic behavior. The A_{2u}(TO) mode is always lower in energy than the corresponding E_u(TO), and the reststrahlen bands always overlap because the A_u(LO) frequency is higher than the E_u(TO) frequency. For a ceramic, the infrared response should be a broad reststrahlen band composed of both the A_{2u} and E_u bands. Figure 4 shows the single-crystal p polarization of this effect, but the s polarization must be superimposed. The s polarization effects gives a band that goes from E_u(TO) to E_u(LO). Thus, for ceramics, a band that starts at A_{2u}(TO) and ends at E_u(LO) is expected. The occurrence of dips in this broad reststrahlen band at A_{2u}(LO) or E_u(TO) will depend on many things, certainly on the sharpness (the damping) of these features.

We believe that the broad highest-frequency reststrahlen band in Sr_2TiO_4 that occurs between 500 and 750 cm^{-1} [Fig. 3(a)] has the characteristics described above. In fact, based on the analogue with the fluoride results shown in Fig. 5, Fig. 4 has been drawn to represent this case. Hence, from the Kramers-Kronig analysis [Figs. 3(b) and 3(c)] of the reflectivity data several modes can be determined. The peak of $\mathrm{Re}(\epsilon)$ gives A_{2u}(TO) mode at 500 cm^{-1} and from the peaks in $\mathrm{Im}(-\epsilon^{-1})$, the A_{2u}(LO) and E_u(LO) are at ≈ 680 cm^{-1} and at 720 cm^{-1}, respectively. We see no signs of the E_u(TO) mode even in low-temperature measurements.

Now we consider the lowest-frequency modes. For some of the fluorides and chlorides (Fig. 5) the two lowest E_u modes are lower in frequency than the lowest A_{2u} mode.[17-20] Also, the second highest E_u mode is a weak infrared mode; it arises from the silent, T_{2u} mode from the oxygen octahedra in the perovskites,[14] which in this structure correlates to an E_u mode and the silent B_{2u} mode [Table I, part (b)]. In the reflectivity results, this causes a particularly sharp, almost resonantlike, dip between the lowest E_u(LO) feature and this second E_u(TO) feature, because they are so close in energy.[18,19] We believe the rather sharp feature in our reflectivity results [Fig. 3(a)] is just this dip. Hence, from the Kramers-Kronig analysis, the two lowest E_u(TO) frequencies are obtained as well as the E_u(LO) mode between them. These frequencies and assignments are listed in Table II, part (b).

We now are left with two A_{2u}(TO) and one E_u(TO) mode to be assigned, as well as their corresponding LO components. These modes are located between the lowest and highest frequency grouping discussed above, and are more difficult to assign because of the overlap effects discussed above. Hence, these assignments are much more tentative. From the reflectivity results in Fig. 3(a), there appear to be two closely spaced TO modes in the frequency region ≈ 250 cm^{-1}, which become even sharper at low temperatures. We assume that the lower one at ≈ 242 cm^{-1} is an A_{2u}(TO) and the higher one at ≈ 259 cm^{-1} is an E_u(TO) mode. This is based on the idea that the E_u spectra will be more dominant than that from the A_{2u} modes because of s-polarization-type effects. By analogy with the fluoride results (Fig. 5), the strong LO feature at ≈ 440 cm^{-1} is probably due to an LO feature from both A_{2u}(LO) and E_u(LO). Hence, these are so listed in Table II, part (b).

C. Normal modes

Extensive calculations have been carried out by Rauh and Geick[17] of the normal modes in K_2ZnF_4. Since the distances within the octahedra are approximately equal, they use a rigid octahedra model. Of course, this is only an approximation, but is a good starting point for both the fluorides and for Sr_2TiO_4. However, it is not a valid assumption when considering $(La_{2-x}Sr_x)CuO_4$ as we discuss later.

Remembering that only O_z and Sr motion takes place in Raman-active modes [Table I, part (b)], and using these calculations[17] as a basis, we discuss the Raman-active modes first. The highest-frequency Raman A_{1g} mode principally involves the light O_z atoms moving along the z axis, with a smaller amount of Sr motion along this axis, out of phase with the O_z motion. The eigenvector of the lower-frequency A_{1g} mode is orthogonal to the motion in the higher-frequency mode so it principally involves motion of the heavier Sr atom along the z axis. While the A_{1g} modes can be thought of as bond-stretching modes, the E_g modes are similar to bond-bending modes, and thus are lower in frequency. Correspondingly, the highest-frequency E_g mode mostly involves O_z motion in the xy plane, while the lower-frequency mode involves mostly Sr motion in the xy plane. Note that all of these motions are similar to the symmetry-adapted vectors listed in Table I, part (b). The lower-frequency A_{1g} mode and higher-frequency E_g mode tend to have similar frequencies [Fig. 2 and Table II, part (a)] and some direct method to distinguish between them is desirable.

The silent B_{2u}-mode motion is completely determined by symmetry. The motion just involves O_x moving in the plus z direction against O_y moving in the minus z direction [Table I, part (b)]. In cubic perovskite materials this mode is threefold degenerate, allowing for the same type of motion, by pairs of oxygen atoms, in the x and y directions. However, the lower symmetry in Sr_2TiO_4 makes this type of oxygen motion in the x and y directions infrared active. This is the second lowest-frequency E_u mode, already discussed because of its sharp resonantlike reflectivity.[17]

Since all of the atoms can move in the modes that are infrared active, the motions are generally more complicated. We will focus on the lowest- and highest-frequency infrared-active modes since they tend to be the simplest to understand in any model. As would be expected, the lowest-frequency mode involves motion primarily of the heavy Sr atoms agains an approximately rigid TiO_6 oc-

tahedron.[17] For the A_{2u} and E_u modes this motion is in the z direction and xy planes, respectively. The highest-frequency A_{2u} motion involves Ti against an approximately rigid octahedron, with the motion necessarily being in the z direction. The highest-frequency E_u mode involves motion in the xy plane of Ti against O_x and O_y.

As has been pointed out,[9] there is an interesting difference between the fluorides and insulating oxides with the K_2NiF_4 structure, and the oxides that are conductors[22] such as La_2NiO_4 and $(La,Sr)_2CuO_4$. The former materials have rigid octahedra in the sense that the Ti–O_z distance is approximately equal to the Ti–O_x distance. In the latter materials the Ni–O_z distance is considerably greater than the Ni–O_x distance,[13] and in $(La,Sr)_2CuO_4$ this distance is further increased.[23] These different distances effects certain force constants, and hence some of the normal modes.

V. COMPARISON WITH $(La_{2-x}Sr_x)CuO_4$

In Fig. 6, our reflectivity measurements for Sr_2TiO_4 and $(La_{2-x}Sr_x)CuO_4$ for two different values of x, are shown. Our results for $(La_{2-x}Sr_x)CuO_4$ appear similar to other published work[24–27] except that we seem to resolve a bit more detail. $(La_{2-x}Sr_x)CuO_4$ is orthorhombic for $x \lesssim 0.05$ at room temperatures,[28] but the effect on the modes appears to be small since the reported spectra[24–27] for both tetragonal and orthorhombic material are similar to our results shown in Fig. 6, as are our measurements for samples with larger x. From these measurements certain aspects of the $(La_{2-x}Sr_x)CuO_4$ results become clearer. We discuss these points and assign some of the modes.

First, consider the high-frequency region, above ≈ 450 cm^{-1}. For Sr_2TiO_4, as discussed above, this reflectivity response consists of a lower-frequency A_{2u} mode and a higher-frequency E_u mode. $(La_{2-x}Sr_x)CuO_4$ might be expected to be less ionic with a smaller effective charge, which will reduce the TO-LO splittings making it easier to identify some of the modes since overlap between the A_{2u} and E_u reststrahlen bands will be decreased. Indeed, this appears to be the case for $x=0$. As can be seen in Fig. 6, the high-frequency composite response in Sr_2TiO_4, when observed in $(La_{2-x}Sr_x)CuO_4$, clearly divides into two, relatively sharp reststrahlen bands. This immediately suggests that the lower one (≈ 510 cm^{-1}) is due to an A_{2u} phonon and that the higher one (≈ 670 cm^{-1}) is due to an E_u phonon. This assignment is confirmed by the results for the $x=0.04$ sample which contains many free electrons. Since this electron plasma is free to move in the xy plane and not in the z direction,[21,22] it couples much more strongly to E_u phonons than to A_{2u} phonons.[21] This happens because for E_u phonons, the atoms vibrate in the xy plane while A_{2u} phonons vibrate along the z direction. This point has been also discussed previously.[24] Thus, the assignment and frequencies (from a Kramers-Kronig analysis) can be obtained, and the mode frequencies from the $x=0$ sample, for the two highest-frequency modes are listed in Table II, part (c).

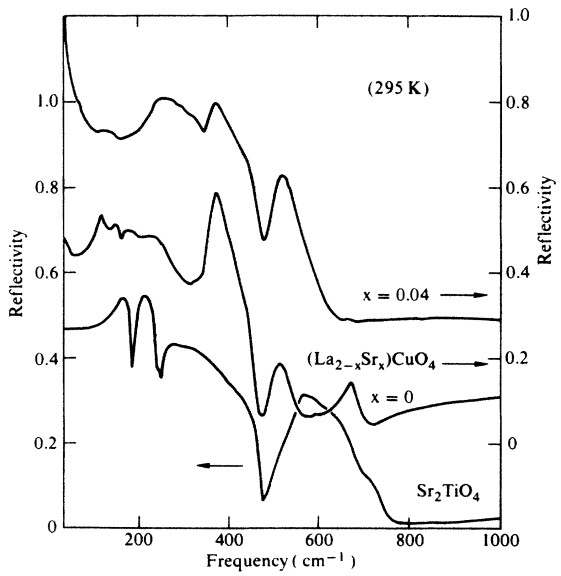

FIG. 6. The frequency dependence of the reflectivity of Sr_2TiO_4 compared t that of $(La_{2-x}Sr_x)CuO_4$ for two different values of x. The reflectivity scale for the latter two materials is shifted for clarity; it is to the right.

Other features for $x=0$ now become clearer. Although this material is actually orthorhombic, we are treating it as if it is tetragonal. The differences between the orthorhombic and tetragonal structure are small,[23] resulting from a soft Brillouin-zone edge phonon.[29] There is no hint of a splitting in the ≈ 650 cm^{-1} reststrahlen feature; yet being a doubly degenerate E_u mode in the tetragonal phase, for an orthorhombic crystal it must split into two singly degenerate modes (transforming as the B_{2u} and B_{3u} irreducible representations of the mmm-D_{2h} point group). Thus, the lower symmetry in $(La_{2-x}Sr_x)CuO_4$ has only a small effect on splitting of the modes from those in the tetragonal phase. The same effect has been noted[10] for orthorhombic $YBa_2Cu_3O_7$, which can be made into tetragonal $YBa_2Cu_3O_6$.

The lowest-frequency feature (≈ 120 cm^{-1}) in the $x=0$ material is probably an E_u mode as in Sr_2TiO_4, the fluorides, and the chlorides (Fig. 5). Again, further evidence for this assignment is obtained from $x=0.04$ sample where the free electrons couple to the E_u modes. For $x=0.04$ there is a small remnant of this feature still observable at the same frequency. Thus, in Table II, part (c) we assign this lowest-frequency mode at 117 cm^{-1} to the E_u(TO) mode obtained from the Kramers-Kronig analysis of either the $x=0$ or 0.04 samples, and the corresponding E_u(LO) mode at ≈ 140 cm^{-1} from the latter sample.

For the $x=0.04$ sample, except for this small feature at ≈ 117 cm^{-1} discussed above, there are three prominent reflectivity bands. We have already assigned the highest-frequency band, starting at 510 cm^{-1} [Table II, part (c)], to an A_{2u} band. We assign the other two features to the allowed A_{2u} phonons. The two highest-frequency A_{2u} bands are clearly visible in the $x=0$ sample, and the lowest A_{2u} band is discernible even though it overlaps with E_u bands, as expected. Frequency values, from a Kramers-Kronig analysis, for these lower-frequency A_{2u} bands, from the $x=0.04$ sample, are listed in Table II,

part (c). However, we are not certain of the lowest-frequency A_{2u}(LO) mode because of the apparent large shift between the $x=0$ and $x=0.04$ sample. Hence, in Table II, part (c) we list this value as (340).

A. Normal modes

There are large relative changes in the $B-O_z$ compared to $B-O_x$ distances in $(La_{2-x}Sr_x)CuO_4$ when compared to the insulating materials. These changes must affect certain eigenvectors. For example, based on the lattice dynamics of the fluorides,[17] in Sr_2TiO_4 the highest-frequency Raman-active A_{1g} eigenvector is principally O_z motion along the z direction with very little Sr motion. The lowest-frequency A_{1g} motion, however, is orthogonal, involving mostly Sr motion. For $(La_{2-x}Sr_x)CuO_4$ this eigenvector must change because of the substantial decrease in the $Cu-O_z$ force constant relative to the O_z-La force constant. Consequently, the highest-frequency A_{1g} motion involves out-of-phase motion of O_z against La along the z direction, while in-phase motion of these two atoms takes place in the lowest-frequency A_{1g} mode. For the highest-frequency E_g modes, the La and O_z will move in the xy plane out of phase with each other. While for the lowest-frequency mode, these two atoms will move in phase. Of course, since the La atom is so much heavier than the O_z atom, it will move much less in these motions.

For the infrared-active $3A_{2u}$ and $4E_u$ modes it is more difficult to generalize because the motion of all the atoms is involved. However, the highest-frequency E_u mode in Sr_zTiO_4 and $(La_{2-x}Sr_x)CuO_4$ should be essentially the same, with the Cu moving against O_x and O_y. The highest-frequency A_{2u} motion in Sr_2TiO_4 is primarily Ti against a rigid oxygen octahedron. However, in $(La_{2-x}Sr_x)CuO_4$ the eigenvector must be rather different because of the relatively stronger forces between $La-O_z$ than between $Cu-O_z$. Some of the lattice dynamical calculations[30-33] come to similar conclusions.

VI. CONCLUSIONS

We have measured the Raman modes and infrared reflectivity in ceramic Sr_2TiO_4, a material that is isostructural with the superconductor $(La_{2-x}Sr_x)CuO_4$. Since the material has a center of symmetry, we expect, and observe, sharp Raman-active modes, and determine all of the four allowed modes. Interpretation of the infrared reflectivity is more difficult since reststrahlen bands extend from the TO to the LO frequency for all $3A_{2u}$ and all $4E_u$ bands. Although all of the $3A_{2u}$ bands must occur in different frequency ranges, as must all $4E_u$ bands, the difficulty in analyzing the data occurs because A_{2u} and E_u bands can overlap each other.

With the help of the single-crystal infrared results in the isostructural fluorides and chlorides, for Sr_2TiO_4 we have been able to assign two E_u modes and one A_{2u} mode, and with less certainty one more of each type. Thus, five out of the seven allowed infrared modes can be assigned using the ceramic samples.

The assignment of modes from the infrared reflectivity measurements in $(La_{2-x}Sr_x)CuO_4$ is easier for two reasons. First, the smaller effective charges reduces the TO-LO splittings. This makes the reststrahlen bands narrower, causing less interference between those of the A_{2u}- and E_u-type bands. Second, the structure has a free-electron-like plasma response only on the xy plane, and not perpendicular to it. Thus, the free electrons couple much more strongly to the E_u phonons, because their motion is also in the xy plane. The free carrier concentration can be increased by increasing x from 0, thereby increasing the plasma frequency, which permits easier observation of all of the $3A_{2u}$ modes (Fig. 6). From the combined spectra for different x, the highest- and lowest-frequency E_u modes also may be identified. Thus, we determine five of the seven infrared-active modes in the superconducting material.

ACKNOWLEDGMENTS

One of us (G.B.) gratefully acknowledges financial support from the Alexander von Humboldt Foundation, and the hospitality and stimulation of colleagues at the Max Planck Institute for Solid State Research where some of this work was carried out. Discussions with Professor E. Burstein, T. Brun, R. E. Cohen, and W. Weber are gratefully acknowledged.

[1] J. G. Bednorz and K. A. Müller, Z. Phys. B **64**, 189 (1986).
[2] For a review of the early work in this field, see A. Khurana, Phys. Today **40** (No. 4), 17 (1987).
[3] Also see A Khurana, Phys. Today **40** (No. 6), 17 (1987).
[4] See most solid state books for a discussion of the Bardeen-Cooper-Shrieffer theory.
[5] For example, see B. P. Schweiss, B. Renker, E. Schneider, and W. Reichardt, in *Superconductivity in d- and f-Band Metals* edited by D. H. Douglass (Plenum, New York, 1976), p. 189.
[6] G. Burns and B. A. Scott, Phys. Rev. Lett. **25**, 167 (1970); G. Burns, Mater. Res. Bull. **6**, 923 (1971).
[7] I. G. Lang and U. S. Pashabekova, Fiz. Tverd. Tela **6**, 3640 (1964) [Sov. Phys. Solid State **6**, 2913 (1965)]; K. R. Allakhverdiev, S. S. Babaev, E. Yu, and M. M. Tagyev, Phys. Status Solidi (b) **96**, 177 (1979).
[8] G. Burns, F. H. Dacol, and M. W. Shafer, Solid State Commun. **62**, 687 (1987).
[9] U. Venkateswaran, K. Strössner, K. Syassen, G. Burns, and M. W. Shafer, Solid State Commun. **64**, 1273 (1987).
[10] G. Burns, F. H. Dacol, P. Freitas, T. S. Plaskett, and W. König, Solid State Commun. **64**, 471 (1987).
[11] S. N. Ruddlesden and P. Popper, Acta Crystallogr. **10**, 538 (1957).
[12] G. J. McCarthy, W. B. White, and R. Roy, J. Am. Ceram. Soc. **52**, 463 (1969).
[13] R. W. G. Wyckoff, *Crystal Structures* (Wiley, New York, 1975), Vol. 3, p. 63; A. F. Wells, *Structural Inorganic Chemistry* (Oxford Univ. Press, New York, 1975); F. S. Glasso, *Structure and Properties of Inorganic Solids* (Pergamon, New York, 1970).

[14]G. Burns and A. M. Glazer, *Space Groups for Solid State Scientists* (Academic, New York, 1978); G. Burns, *Introduction to Group Theory with Applications* (Academic, New York, 1977).

[15]*International Tables for X-ray Crystallography,* edited by N. F. M. Hendry and K. Lonsdale (Kynoch, London, 1952, 1965, 1968), Vol. I.

[16]D. J. Tomes, W. O'Sullivan, and H. J. Guggenheim, Solid State Commun. **14**, 715 (1974); M. Kaneko, G. Kuwabara, and A. Misu, *ibid.* **18**, 1085 (1976).

[17]H. Rauh and R. Geick, Phys. Status Solidi (b) **127**, 55 (1985).

[18]H. Büger, K. Strobel, R. Geick, and W. Müller-Lierheim, J. Phys. C **9**, 4213 (1976).

[19]K. Strobel and R. Geick, J. Phys. C **15**, 2105 (1982).

[20]H. Rauh, R. Geick, N. Lehner, J. Bouillot, and G. Eckold, Phys. Status Solidi (b) **115**, 463 (1983).

[21]J. M. Bassat, P. Odier, and F. Garvais, Phys. Rev. B **35**, 7126 (1987).

[22]C. N. R. Rao, D. J. Buttrey, N. Otsuka, P. Ganguly, H. R. Harrison, C. J. Sandberg, and J. M. Honig, J. Solid State Chem. **52**, 266 (1984).

[23]R. J. Cava, A. Santoro, D. W. Johnson, Jr., and W. W. Rhodes, Phys. Rev. B **35**, 6716 (1987); P. Day, M. Rosseinsky, K. Prassides, W. I. F. David, O. Moze, and A. Soper, J. Phys. C **20**, L429 (1987).

[24]Z. Schlesinger, R. T. Collins, and M. W. Shafer, Phys. Rev. B **35**, 7232 (1987).

[25]D. A. Bonn, J. E. Greedan, C. V. Stager, T. Timusk, M. G. Doss, S. L. Herr, K. Kamaras, C. D. Porter, D. B. Tanner, J. M. Tarascon, W. R. McKinnon, and L. H. Greene, Phys. Rev. B **35**, 8843 (1987).

[26]H. P. Geserich, G. Scheiber, and B. Renker, Solid State Commun. **63**, 657 (1987).

[27]S. Sugai, S. Uchida, H. Takagi, K. Kitazawa, and S. Tanaka, Jpn. J. Appl. Phys. **26**, L879 (1987).

[28]R. M. Fleming, B. Batlogg, R. J. Cava, and E. A. Rietman, Phys. Rev. B **35**, 13 (1987); K. Kang, G. Collin, M. Ribault, J. Friedel, J. Jerome, J. M. Bassat, J. P. Coutoures, and Ph. Odier, J. Phys. (Paris) **48**, 1181 (1987).

[29]R. J. Birgeneau, C. Y. Chen, D. R. Gabbe, H. P. Jenssen, M. A. Kastner, C. J. Peters, P. J. Picone, Tineke Thio, T. R. Thurston, H. L. Tuller, J. D. Axe, P. Boni, and G. Shirane, Phys. Rev. Lett. **59**, 1329 (1987).

[30]T. Brun, M. Grimsditch, K. E. Gray, R. Bhadra, and V. Maroni, Phys. Rev. B **35**, 16 (1987).

[31]W. Weber, Phys. Rev. Lett. **58**, 1371 (1987).

[32]R. E. Cohn, W. E. Pickett, H. Krakauer, L. L. Boyer, Physica B (to be published).

[33]J. Prade, A. D. Kullkarni, F. W. de Wette, W. Kress, M. Cardona, R. Reiger, and U. Schröder, Solid State Commun. (to be published).